Biogeosciences Open Access
Discussions
EGU

Quantifying impacts of the drought 2018 on European ecosystems in comparison to 2003

Allan Buras[1], Anja Rammig[1], Christian S. Zang[1]

[1]Land Surface Atmosphere Interactions, Technical University of Munich, TUM School of Life Sciences Weihenstephan, Hans-Carl-von-Carlowitz Platz 2, 85354 Freising, Germany.

Correspondence to: Allan Buras (allan@buras.eu)

Abstract. In recent decades, an increasing persistence of atmospheric circulation patterns has been observed. In the course of the associated long-lasting anticyclonic summer circulations, heat waves and drought spells often coincide, leading to so-called hotter droughts. Previous hotter droughts caused a decrease in agricultural yields and increase in tree mortality, and thus, had a remarkable effect on carbon budgets and negative economic impacts. Consequently, a quantification of ecosystem responses to hotter droughts and a better understanding of the underlying mechanisms is crucial. In this context, the European hotter drought of the year 2018 may be considered as a key event. As a first step towards the quantification of its causes and consequences, we here assess anomalies of atmospheric circulation patterns, temperature loads, and climatic water balance as potential drivers of ecosystem responses which are quantified by remote sensing using the MODIS vegetation indices NDVI and EVI. To place the drought of 2018 within a climatological context, we compare its climatic features and remotely sensed ecosystem response with the extreme hot drought of 2003. 2018 was characterized by a climatic dipole, featuring extremely hot and dry weather conditions north of the Alps but comparably cool and moist conditions across large parts of the Mediterranean. Analysing ecosystem response of five dominant land-cover classes, we found significant positive effects of April-July climatic water balance on ecosystem productivity. Negative drought impacts appeared to affect a larger area and to be significantly stronger in 2018 compared to 2003. Moreover, we found a significantly higher sensitivity of pastures and arable land to climatic water balance compared to forests in both years. The stronger coupling and higher sensitivity of ecosystem response in 2018 we explain by the prevailing climatic dipole: while the generally water-limited ecosystems of the Mediterranean experienced above-average climatic water balance, the less drought-adapted ecosystems of Central and Northern Europe experienced a record hot drought. In conclusion, this study quantifies the drought of 2018 as a yet unprecedented event, outlines hotspots of drought-impacted areas in 2018 which should be given particular attention in follow-up studies, and provides valuable insights into the heterogeneous responses of the dominant European ecosystems to hotter drought.

30

Biogeosciences
Discussions

EGU Open Access

1 Introduction

More frequent and longer-lasting heat waves are expected to occur with global warming (IPCC, 2014). If such heat waves coincide with low precipitation sums, so-called 'global-change type droughts' or 'hotter droughts' emerge (Allen et al., 2015;
35 Breshears et al., 2005). In the course of hotter droughts, positive feedback loops related to a non-linearly amplified soil-water depletion through evapotranspiration (Seneviratne et al., 2010) further aggravate surface-temperature anomalies because of reduced latent cooling (Fischer et al., 2007). To emphasize this interdependence of heat and drought and improve projections of potential high-impact events, hotter droughts were recently classified as compound events (Zscheischler et al., 2018). Accounting for the interdependence of climatic drivers for drought, climate model projections generally indicate an increase
40 in the likelihood of a hotter drought during the 21st century (Zscheischler and Seneviratne, 2017). Given the associated climatic properties, hotter droughts are more likely to occur under abnormally stable anticyclonic atmospheric circulation patterns which were recently shown to be connected with a hemisphere-wide wavenumber 7 circulation pattern (Kornhuber et al., 2019). Abnormally stable anticyclonic atmospheric circulation patterns and associated wavenumber 7 circulation patterns have expressed an increasing frequency over the past decades (Horton et al., 2015; Kornhuber et al., 2019).

45 Hotter droughts feature a wide range of negative impacts on managed and natural ecosystems, e.g. reduced productivity, as indicated by lower vegetation greenness using remote sensing data (Allen et al., 2015; Choat et al., 2018; Ciais et al., 2005; Orth et al., 2016; Xu et al., 2011). As a consequence, agricultural yields decline remarkably during hotter droughts while drought-induced tree mortality increases, with both effects leading to significant economic losses (Allen et al., 2010; Buras et al., 2018; Cailleret et al., 2017; Choat et al., 2018; Ciais et al., 2005; Matusick et al., 2018). Moreover, since gross primary
50 productivity (GPP) decreases during hotter droughts, the resulting lower net carbon uptake may change ecosystems from carbon sinks into carbon sources (Ciais et al., 2005; Xu et al., 2011). However, the response to drought may vary among different land-cover types, particularly between grasslands and forests (Teuling et al., 2010; Wolf et al., 2013).

On the continental scale, the European heat wave of 2003 is to date considered as the most extreme compound event in Europe over the last century with various impacts on human health (increased mortality particularly in France), economy (decreased
55 crop yield in agriculture and forestry), and ecosystems (reduced productivity, forest die-back, and an increased frequency of forest fires; Fink et al., 2004; García-Herrera et al., 2010). According to Ciais et al. (2005), GPP of European ecosystems was reduced by 30 percent in summer 2003 – a yet unprecedented reduction in Europe's primary productivity which resulted in an estimated net carbon release of 0.5 PG C yr^{-1}. Given the wide-ranging impacts, potential climate change feedback loops, and the increasing frequencies of circulation patterns initiating compound events it is pivotal to better understand and thus more

Biogeosciences Discussions

60 precisely predict the response of managed and natural ecosystems to hotter droughts (Horton et al., 2015; Pfleiderer and Coumou, 2018; Sippel et al., 2017; Zscheischler and Seneviratne, 2017).

In the context of an increased persistence of circulation patterns, the European drought of 2018 is of particular interest. In April 2018, a high-pressure system established over Central Europe and persisted almost continuously until mid of October, thereby causing a long-lasting drought spell and record temperatures in central and northern Europe. Despite preliminary reports in

65 public news and the world-wide-web (see list of public news references), the direct impacts resulting from the 2018 drought are still unexplored. Consequently, we here quantify the impacts of the extreme drought of 2018 on European ecosystems in comparison to the extreme drought in the year 2003. Thereby, we 1) provide an estimate of European ecosystems immediate response to the drought 2018 in relation to 2003, 2) identify hotspots of extreme drought and associated ecosystem response, and 3) aim at an improved mechanistic understanding of the processes driving ecosystem responses to extreme drought events.

70 **2 Material and Methods**

2.1 Data sources and preparation

2.1.1 Climate data

To visualize the general circulation patterns in 2003 and 2018 we downloaded gridded reanalysis data representing 500 hPa geopotential height from the NCEP/NCAR Reanalysis project provided by the NOAA climate prediction center (Kalnay et al.,

75 1996) available at the Earth System Research Laboratory (ESRL, https://www.esrl.noaa.gov/). The downloaded data cover the period 1981-2018 at a daily temporal resolution and a spatial resolution of 2.5°. As a representation of high-pressure persistence, we computed the mean geopotential height for each grid cell and year for the period from 1st of April until 31st of July.

From ESRL, we furthermore downloaded reanalyzed (NCEP/NCAR), daily gridded mean minimum and maximum

80 temperature (Tmin, Tmax) and precipitation (P) sums at 0.5° spatial resolution covering the period 1981-2018 (Kalnay et al., 1996). These variables were used to compute potential evapotranspiration (PET, as defined by Hargreaves, 1994) and the climatic water balance (CWB = P-PET, Thornthwaite, 1948). As for geopotential height, we for each grid cell and year integrated Tmax and CWB for the period from 1st of April until 31st of July as measures of heat load and water balance.

Processed climate data were spatially truncated to match the region considered for the MODIS satellite images (see next

85 section) resulting in 2312 climate grid cells representing an area of roughly 5.9 million km² and covering 38 years. To allow for combination with MODIS data throughout the analyses, processed climate data were re-projected to MODIS native projection using zonal means while retaining a spatial resolution of 0.5°.

2.1.2 MODIS vegetation indices

90 Using the Application for Extracting and Exploring Analysis Ready Samples (AppEEARS; https://lpdaacsvc.cr.usgs.gov/appeears) we downloaded two MODIS vegetation indices (VI, i.e. the Normalized Difference

Vegetation Index NDVI and the Enhanced Vegetation Index EVI) and the corresponding pixel reliability layers at 231 m spatial resolution and 16 days temporal resolution in their native projection. The downloaded data cover the area between 10° E and 30° W longitude, 36.5° N and 71.5° N latitude that is represented by the CORINE land cover information of 2012

95   (see section 2.1.3) and span the period from February 2000 until end of 2018.

Based on the pixel reliability information, we only retained records with good or marginal quality for subsequent analyses. Consequently, for most of the grid cells the VI time series contained missing values due to temporary clouds or snow cover. If the number of missing values was larger than the number of VI records, we considered the representing records as insufficient for our analyses and consequently removed the corresponding pixel from the analysis. However, since high-elevation as well

100   as high-latitude pixels had many missing values in winter and spring because of clouds and snow cover and we only were interested in VI during peak season, we only considered the period from beginning of March (DOY 64) to end of October (DOY 304) for the definition of valid pixels. Following these selection criteria, we retained 95,523,236 pixels for the final analyses, representative of an area of 5,970,202 km².

Prior to the analyses, VI time series of the retained pixels were further processed. We linearly interpolated the missing values

105   of the corresponding VI time series for each pixel using the previous and succeeding records (Misra et al., 2016, 2018). Subsequently, we removed negative outlier values from each VI time series by computing standardized residuals to a Gaussian-filtered (filter size of 80 days, i.e. 5 MODIS time steps), smoothed time-series. Residuals exceeding two negative standard deviations were replaced by the equivalent value of the smoothed time series (see also Misra et al., 2018, 2016). We smoothed the interpolated, outlier-corrected time series by reapplying the Gaussian filter. This procedure was necessary to efficiently

110   handle the remaining high-frequency variability in the seasonal VI-cycle (Misra et al., 2016, 2018).

Finally, VI time series were detrended for each pixel individually by determining the linear trend of VI for each pixel and subtracting the pixel-specific trend from the corresponding pixel. This detrending was necessary to compensate trends that were reported for vegetation indices (Bastos et al., 2017) which were also apparent in the downloaded data (Fig. S1). A comparison between non-detrended and detrended data revealed similar spatial patterns with respect to between-pixel

115   variability, however with amplified differences between 2003 and 2018 in the raw, non-detrended data. That is, for the raw data, the observed trend caused in dependence of its sign lower or higher peak-season VI values in 2003 compared to 2018, thereby introducing an offset between these two drought events. Concluding, the detrending was able to efficiently handle the varying VI-trends over the MODIS-era, while spatial patterns were generally retained.

Both NDVI and EVI are considered as proxy for photosynthetic carbon fixation, and thus allow for assessing possible changes

120   in productivity in dependence of environmental conditions (Huete et al., 2006; Myneni et al., 1995; Xu et al., 2011). Moreover, NDVI has earlier been used in the context of drought monitoring (Anyamba and Tucker, 2012). For reasons of simplicity, we focus on results derived from NDVI which are generally confirmed by results derived from EVI as shown in the supplementary information.

125

Biogeosciences
Discussions

2.1.3 CORINE land cover information

To get an impression on the drought-impact on key European ecosystem components, analyses were stratified using the Coordinated Information on the European Environment land cover map (CORINE, https://land.copernicus.eu/pan-
130 european/corine-land-cover/clc-2012) at MODIS resolution. The land cover map was re-projected (as were the gridded climate data) to MODIS native projection using the nearest neighbour method, thereby retaining the original land-cover classes. Given their dominance in Europe and their importance for land-use, we constrained this stratification to pastures, arable land, as well as coniferous, mixed, and broadleaved forests.

135 ## 2.2 Statistical analyses

To quantify weather conditions for the years 2003 and 2018 in relation to average conditions, standardized anomalies of 500 hPa geopotential height, heat load, and CWB were calculated. Before doing so, we tested the underlying assumption of normal distribution by computing Shapiro test for each grid cell and climate parameter respectively (Fig. S2). The number of significant tests ($p < 0.001$) indicating non-normal distribution was in the order of expected false positives (0.0-0.3 percent vs.
140 0.1 percent type I error probability). Therefore, we considered the assumption of normality to be fulfilled. To derive anomalies, we first computed the mean and standard deviation for all variables for the full period (1981-2018). Subsequently, we for 2003 and 2018 determined the difference of the respective metric to its corresponding mean in units of standard deviations which in the following are called standardized anomalies (this procedure is also known as z-transformation). Thus, for integrated geopotential height, heat load, and CWB we obtained each one standardized anomaly per grid cell for 2003 and 2018. The
145 resulting standardized anomalies were mapped and statistically evaluated using histograms. Histograms were used to depict the absolute area representing climate anomalies in 2003 and 2018 which were compared among each other as well as to a normal distribution as a representation of conditions as expected in normal years.

To quantify the response of European ecosystems to the two drought events, we focused on end-of-July (DOY 209) VI values. The selection of this particular date represents a compromise between proximity to peak-season (end of June, before maximum
150 temperatures had been reached) and the occurrence of heat-waves (end of July to mid of August). Since VI features a bounded distribution (values between -1 and +1), we could not apply a standardization approach as for the climate variables. Therefore, we computed for each VI time series its end-of-July quantiles over the 19 years similar to Orth et al. (2016). The corresponding quantiles were mapped for 2003 and 2018. Areas representing the 19 different quantiles were extracted and compared between 2003 and 2018 in a histogram. To depict the temporal development of drought responses in 2003 and 2018, corresponding VI
155 quantiles of areas featuring a CWB anomaly lower than -2 were averaged for each time-step (beginning on January 1st with 16 days interval) and visually compared to each other.

Since we were aiming at a better understanding of particular ecosystems' response to drought severity, we subsequently pooled VI quantiles according to three classes of CWB anomalies (abnormal water deficit: CWB < -2, average water supply: -2 < CWB < 2, abnormal water surplus: CWB >2) and five CORINE land-cover classes (arable land, pastures, coniferous forest,

160   mixed forest, broadleaved forest). For the resulting 15 combinations, we again compared the areas representing the 19 different quantiles between 2003 and 2018 as done for the total scene. Since the areas of CWB-land cover combinations differed between 2003 and 2018, we moreover computed histograms expressing proportional areas for 2003 and 2018.

Finally, we aimed at developing empirical relationships between CWB anomalies and VI quantiles for the five CORINE land-cover classes mentioned before. For this, we logit transformed VI-quantiles (quantiles ranging from 0 to 1) to obtain an
165   unbounded distribution and subsequently extracted the corresponding mean of transformed VI-quantiles for each CWB grid-cell (thus n = 2312). To assess the effect of different land cover classes, we extracted both the mean EVI-quantiles representing all five land cover classes as well as for each land cover class separately. For the corresponding 2312 CWB-pixels we computed linear regressions between the transformed EVI-quantiles as the dependent variable and CWB anomalies as independent variable separately for 2003 and 2018 and for the six different land cover types (i.e. five separate classes as well as their
170   combination).

For linear regression evaluation, we report adjusted r² and display scatterplots of logit-transformed VI quantiles vs. CWB along with the corresponding regression line. Moreover, regression slopes were compared statistically for each land cover type between 2003 and 2018. For this, each slope estimate was bootstrapped using random subsampling over 1000 iterations and the overlap of 95 % confidence intervals was evaluated. That is, in case the confidence intervals of a respective comparison
175   did not overlap, we considered the difference between slopes as significant. In a similar manner, we compared model slopes among ecosystems (i.e. pastures, arable land, as well as coniferous, mixed, and deciduous forest) separately for 2003 and 2018. Model slopes were grouped according to their overlap of 99.9 % confidence intervals. Finally, to backup observations made from our analyses we also computed a global model (n = 4624) by applying a linear mixed effects model (lme) to EVI quantiles using climatic water balance as fixed effect and incorporating crossed random slopes of land cover and year. All analyses were
180   performed in 'R' (R core team, 2019) extended for the packages, 'nlme' (Pinheiro et al., 2017), 'raster' (Robert J. Hijmans, 2017), and 'SPEI' (Beguería and Vicente-Serrano, 2013).

3 Results

All considered climate parameters indicated abnormal weather conditions for 2018 (Figs. 1-3). The integrated 500 hPa
185   geopotential height, an indicator of the persistence of the atmospheric circulation, expressed anomalies in the order of two positive standard deviations for large parts of Central and Northern Europe, mainly covering the Baltic Sea region (Fig. 1 b). In comparison, 2018 differed from 2003 by featuring a dipole of 500 hPa geopotential height anomalies. While in 2003 most of Europe featured strong positive anomalies, the Mediterranean was characterized by low geopotential height anomalies in 2018 (Fig. 1 a vs. Fig. 1 b). The observed dipole of 2018 expressed a bimodal distribution of anomalies, while 2003 featured
190   a skewed distribution towards positive anomalies (Fig. 1c). Consequently, in 2018 the area featuring positive anomalies was 0.55% of the area in 2003, i.e. 3.1 million km² vs. 5.7 million km² in 2003. At the same time, the area with negative anomalies was 3.7 times higher in 2018, i.e. 3.5 million km² in 2018 vs. 0.9 million km² in 2003 (Fig. 1c).
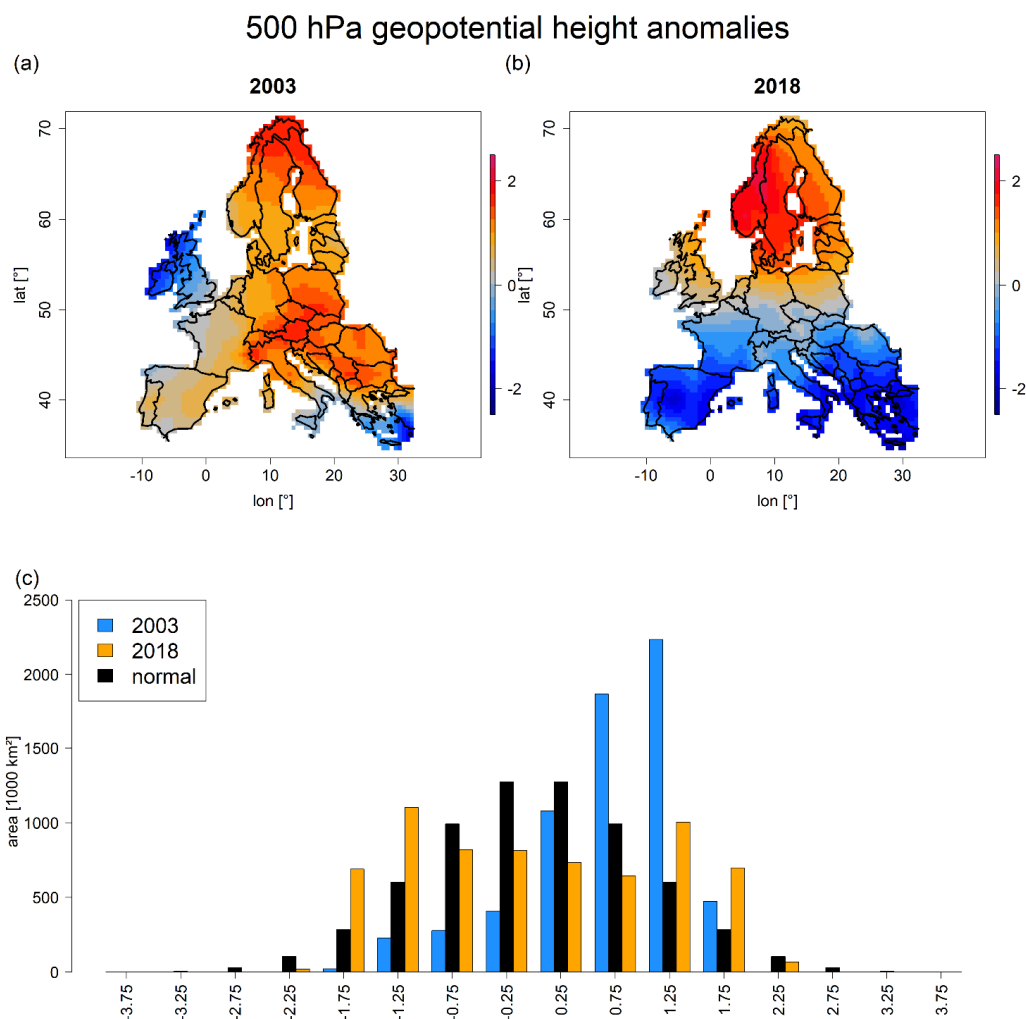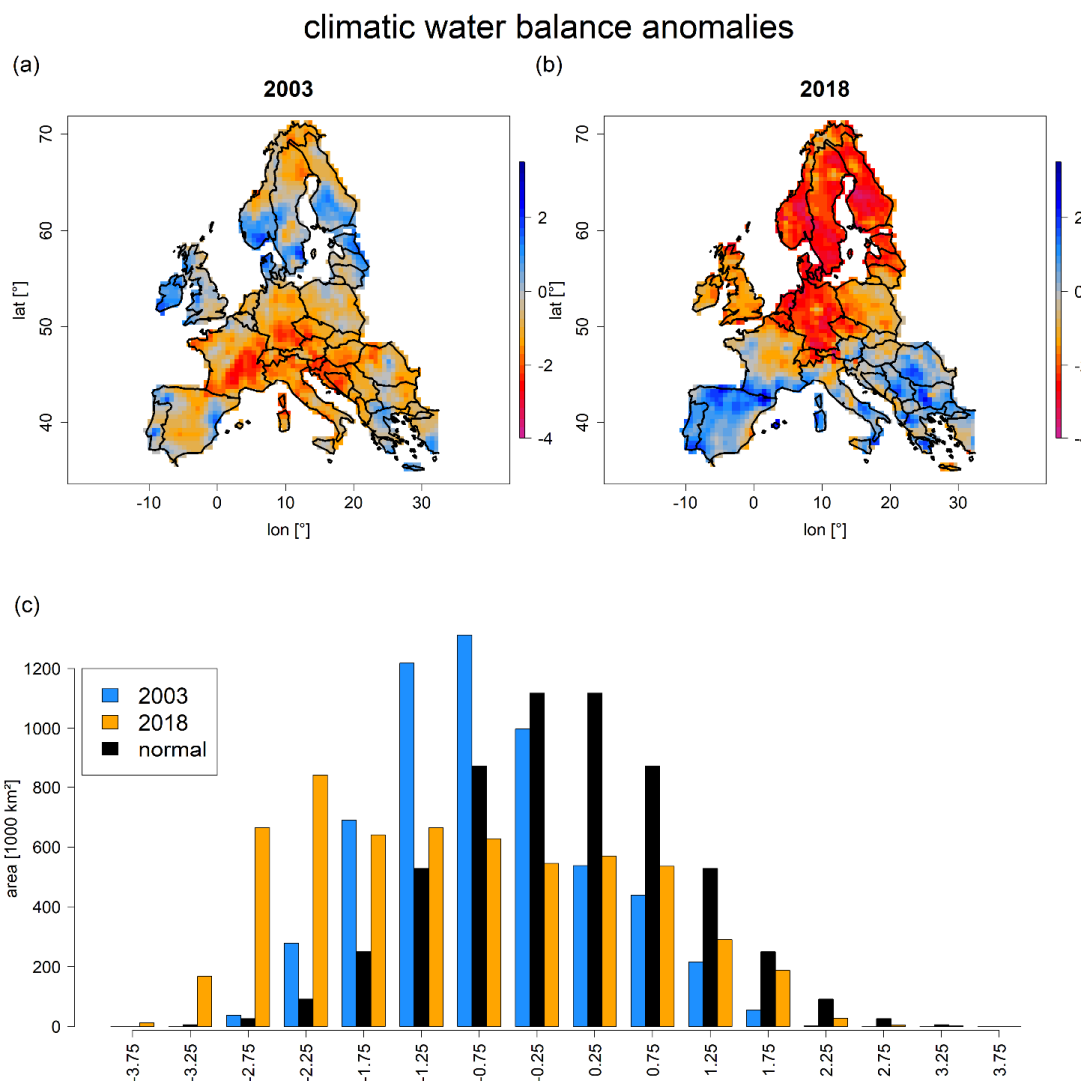
Figure 1: Maps depicting standardized anomalies of April-July 500 hPa geopotential height for 2003 and 2018 (a, b) as well as corresponding area histograms (in units of 1000 km²) for 2003 (blue), 2018 (orange), compared to a normal distribution (black) (c). Blue colours in (a) and (b) indicate geopotential height lower than average, whereas red colours indicate above average geopotential height in comparison to the 1981-2018 mean.

Heat-load anomalies revealed up to four positive standard deviations (i.e. extreme heat) over large parts of Central and Northern Europe in 2018 (Fig. 2 b). In contrast, the Mediterranean featured average conditions (i.e. slightly warmer or cooler) and strong negative anomalies on the Iberian Peninsula. Although the total area with positive heat-load anomalies was more or less similar in 2003 and 2018 (Fig. 2b vs. 2a), anomalies above two positive standard deviations covered a 7.1 times larger area in 2018, i.e. 3.3 million km² vs. 0.5 million km² in 2003 (Fig. 2c). Most contrasting differences between 2003 and 2018 were observed in Southern Italy (hot in 2003, cool in 2018) as well as Scandinavia and the Baltic Sea region (cool in 2003, hot in 2018).
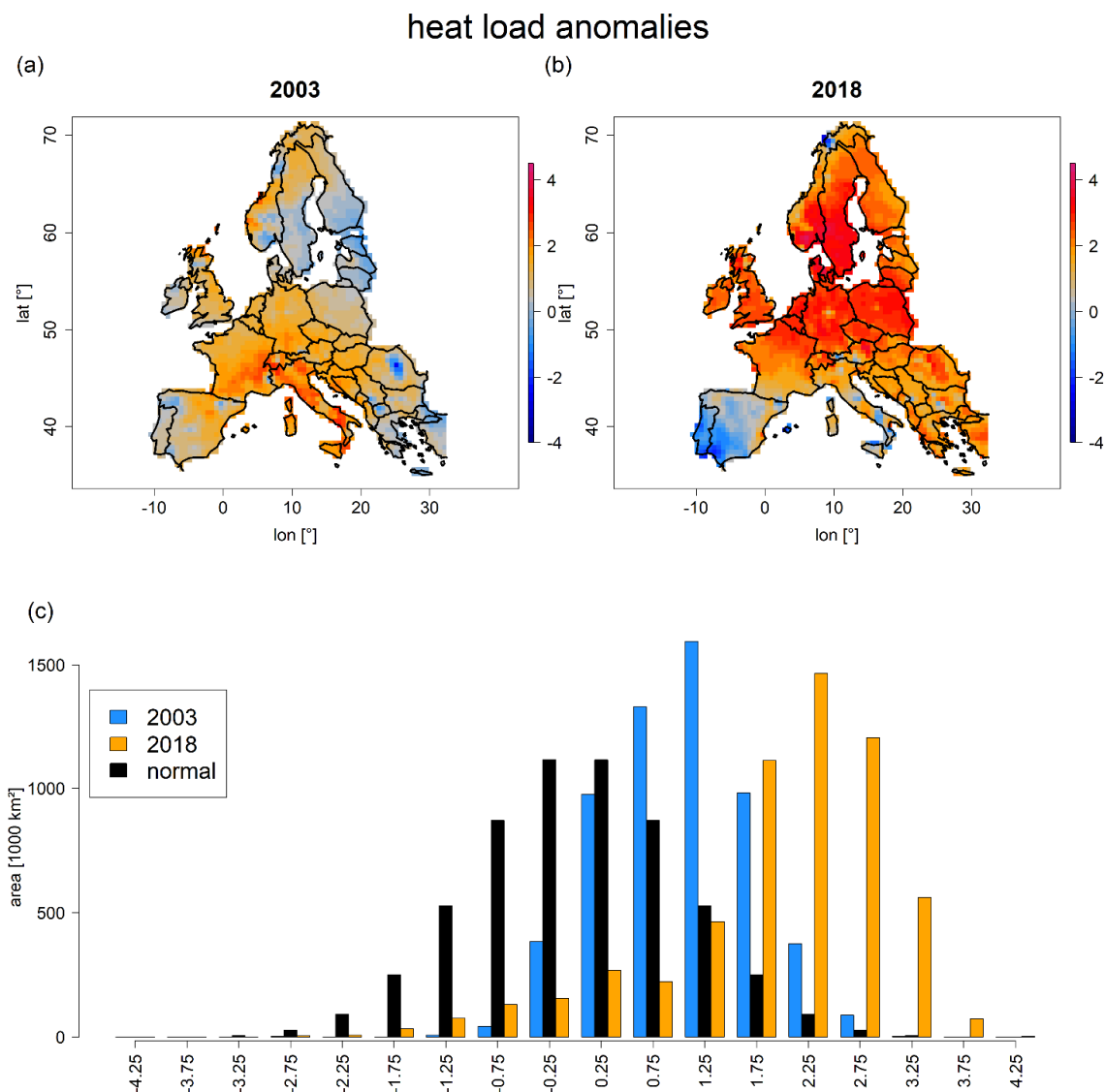
Figure 2: Maps depicting standardized anomalies of April-July heat load for 2003 and 2018 (a, b) as well as corresponding area histograms (in units of 1000 km²) for 2003 (blue), 2018 (orange), compared to a normal distribution (black) (c). Blue colours in (a) and (b) indicate relatively cool conditions, whereas red colours indicate warmer conditions in comparison to the 1981-2018 mean.

CWB for 2018 revealed patterns largely consistent with heat load (Fig. 3b). Again, Central and Northern Europe featured extreme negative (thus dry) deviations, while the Mediterranean generally expressed positive (thus moist) deviations. In comparison (Fig. 3b vs. 3a), the area with negative (i.e. dry) CWB anomalies was relatively similar in both years (Fig. 3c). However, if considering CWB anomalies below two negative standard deviations (i.e. extreme drought), in 2018 an area 5.3 times larger than in 2003 was affected, i.e. 1.7 million km² in 2018 in vs. 0.3 million km² in 2003 (Fig. 3c).

8

Figure 3: Maps depicting standardized anomalies of April-July climatic water balance for 2003 and 2018 (a, b) as well as corresponding area histograms (in units of 1000 km²) for 2003 (blue), 2018 (orange), compared to a normal distribution (black) (c). Blue colours in (a) and (b) indicate relatively moist conditions, whereas red colours indicate dryer conditions in comparison to the 1981-2018 mean.

End of July vegetation response indicated clear differences between 2003 and 2018. We found low NDVI quantiles in large parts of Central Europe, Southern Scandinavia, and the Baltic Sea region and high quantiles in the Mediterranean in 2018 (Fig. 4b). In comparison, 2003 featured low NDVI quantiles in Western, Central, and Southeast Europe and high quantiles in Northern Europe (Fig. 4a). The most prominent difference between 2018 and 2003 was the 2 times larger area featuring the lowest quantile, i.e. 822,067 km² in 2018 vs. 408,614 km² in 2003 (Fig. 4c). At the same time, a 2 times larger area featured

the highest quantile in 2018, i.e. 439,460 km² vs. 214,922 km² in 2003 (Fig. 4c). According to NDVI quantiles, hotspots of

230 drought-response in 2018 were located in Ireland, United Kingdom, France, Belgium, Luxemburg, the Netherlands, Northern Switzerland, Germany, Denmark, Sweden, Southern Norway, Czech Republic, Poland, Lithuania, Latvia, Estonia, and Finnland.
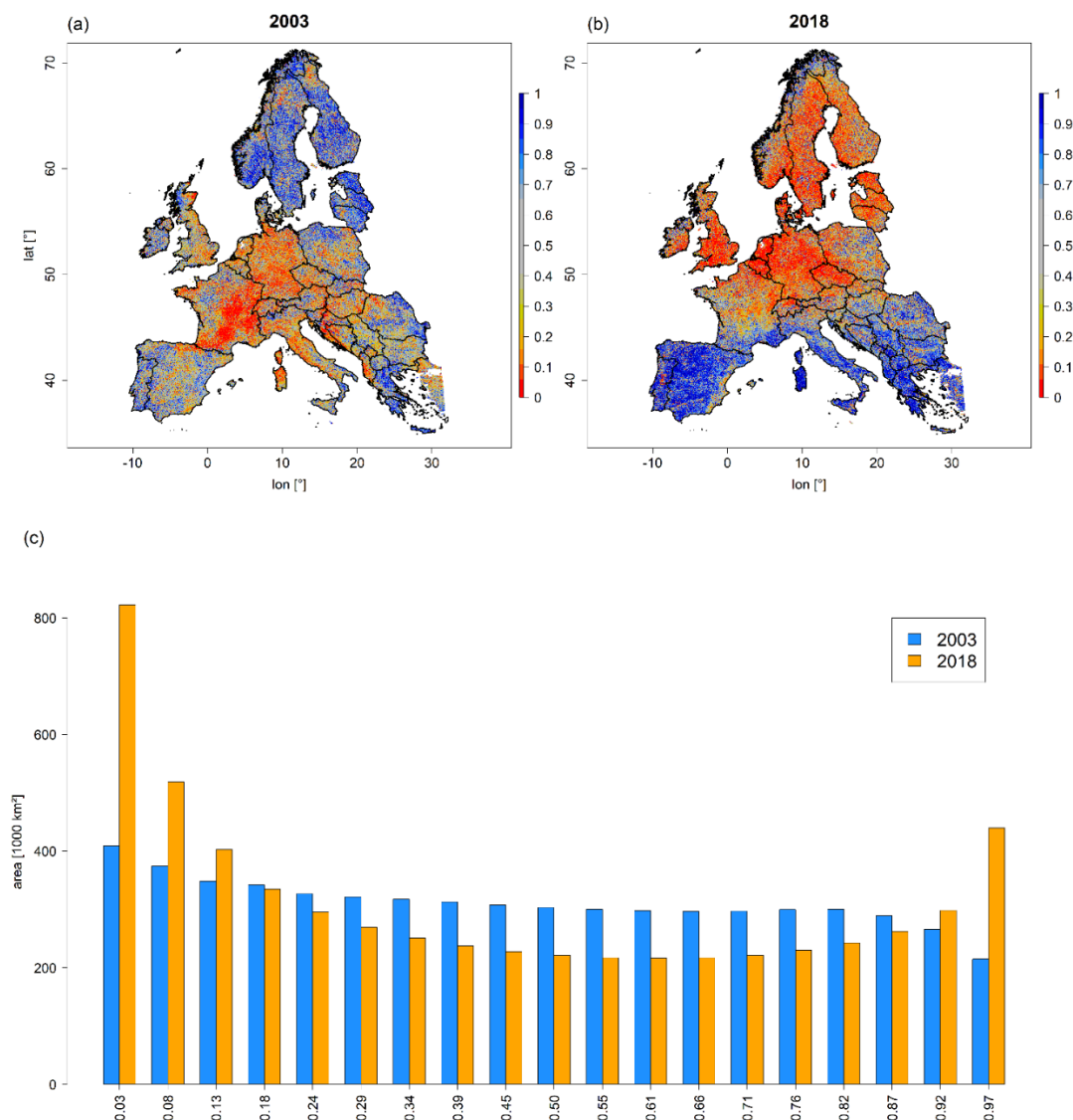
Figure 4: MODIS NDVI quantiles representing peak-season conditions at the end of July (DOY 209) in 2003 (a) and 2018 (b) as well
235 **as the corresponding area histograms (in units of 1000 km²) representing the nineteen NDVI quantiles (c). Blue colours in (a) and (b) indicate upper quantiles (thus a higher than average vegetation greenness), while orange to red colours indicate lower anomalies (i.e. lower than average vegetation greenness). Blue bars in (c) refer to 2003 and orange bars to 2018. Complementary results for MODIS EVI are shown in supplementary Fig. S4.**

240   In regions with water deficit (CWB anomalies below - 2 SD; Fig. 5c) we found a higher frequency of low NDVI quantiles compared to upper quantiles. Similarly, regions with water surplus (CWB anomalies above > 2 SD; Fig. 5a) featured higher frequencies for upper quantiles compared to lower quantiles which however was more pronounced in 2018 compared to 2003. Interestingly, normal conditions (Fig. 5b) featured an inconsistent picture for the different land-cover classes in both years. The most prominent difference was related to absolutely larger areas being affected by water deficit and surplus in 2018

245   compared to 2003. If considering relative frequencies, histograms of 2018 and 2003 became more similar but yet revealed a higher proportion of negatively affected coniferous and mixed forests in 2018 (Fig. S3).

The temporal development of NDVI quantiles from the drought regions was rather similar between 2018 and 2003 (Fig. 6). On average, time series featured lowest quantiles around DOY 209. Most prominent differences between the two events were observed for coniferous and mixed forests, which revealed lower mean quantiles in 2018 while the negative peak of quantiles

250   appeared to occur later for pastures and arable land in 2003.

The impression of CWB affecting NDVI quantiles was underpinned by the linear regressions between the logit-transformed NDVI quantiles and the CWB-anomaly in 2003 and 2018, respectively (Fig. 7a-f). For all land-cover classes a significant and positive effect of climatic water balance on NDVI quantiles was observed, particularly in 2018. Explained variance (r^2) and bootstrapped model slopes were consistently higher in 2018 compared to 2003 (Fig. 7g). In addition, r^2 and model slopes were

255   in both years highest for pastures, followed by arable land, and the three forest types which did not differ among each other (lower case letters in Fig. 7g). The linear mixed effects model over all land-cover classes and the two years confirmed the significant fixed effect of climatic water balance on logit-transformed NDVI quantiles (marginal r^2 = 0.47). Incorporation of random slopes related to land cover and year increased explained variance by 9 percent (conditional r^2 = 0.51), confirming the varying effect of the two drought events as well as the differing impact on different land-cover classes. All presented results

260   based on NDVI are generally confirmed by complementary analyses using EVI (supplementary Figs. S4-S7).
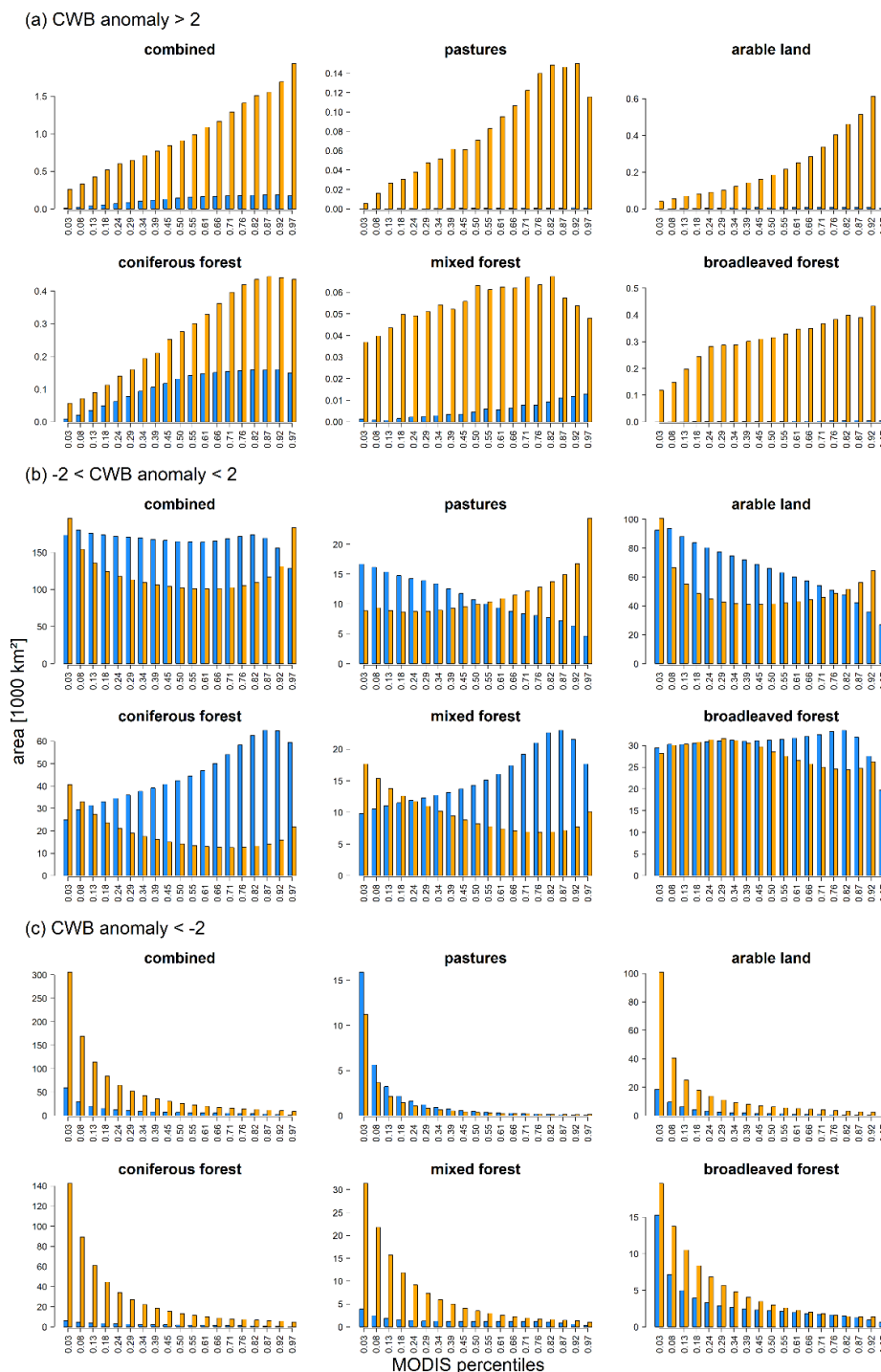
Figure 5: Histograms depicting the absolute areas (in units of 1000 km²) representing the nineteen NDVI quantiles pooled according to CORINE land-cover classes for regions that featured (a) water surplus (CWB-anomaly > 2), (b) average conditions (- 2 < CWB-anomaly < 2), and (c) water deficit (CWB-anomaly < -2). Blue bars refer to 2003, orange bars to 2018. Histograms depicting the proportional areas are shown in supplementary Fig. S3, results for MODIS EVI in supplementary Figs. S5 and S6.
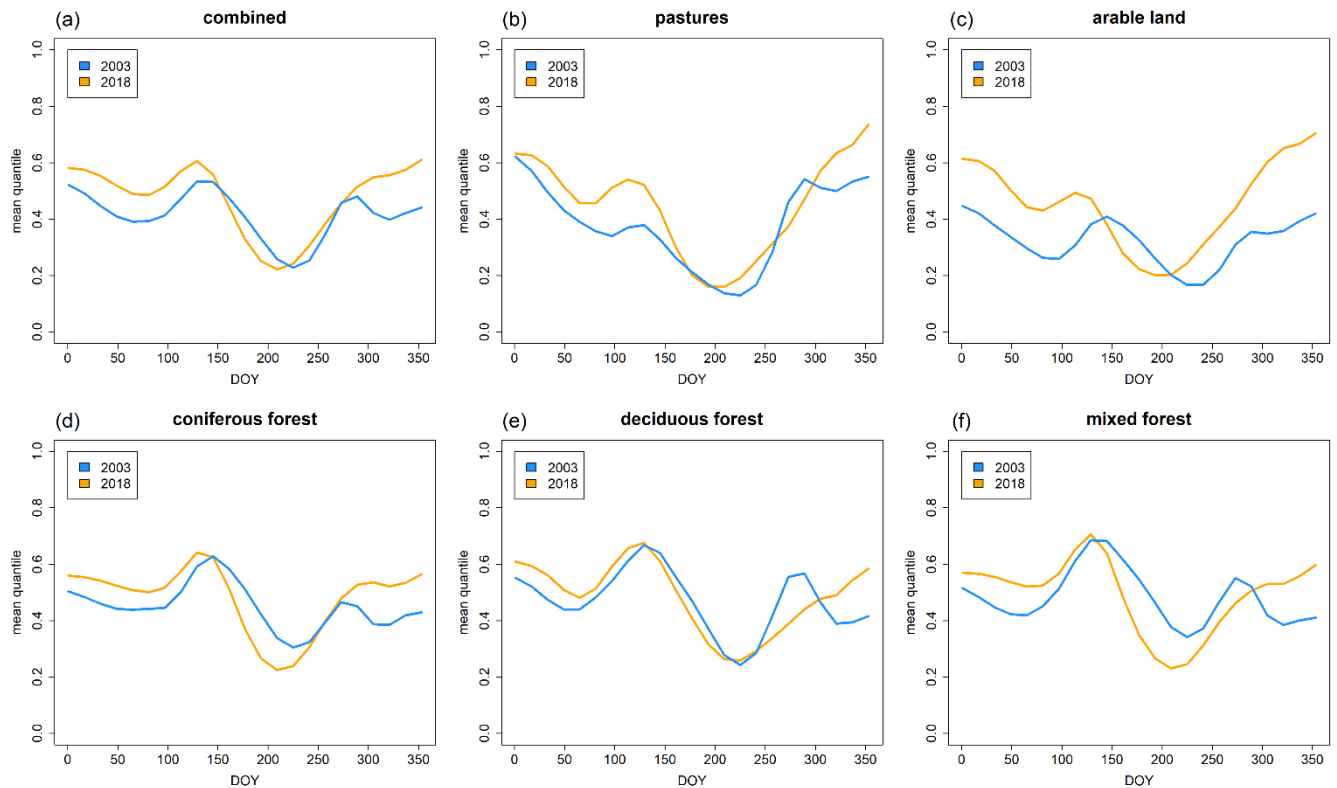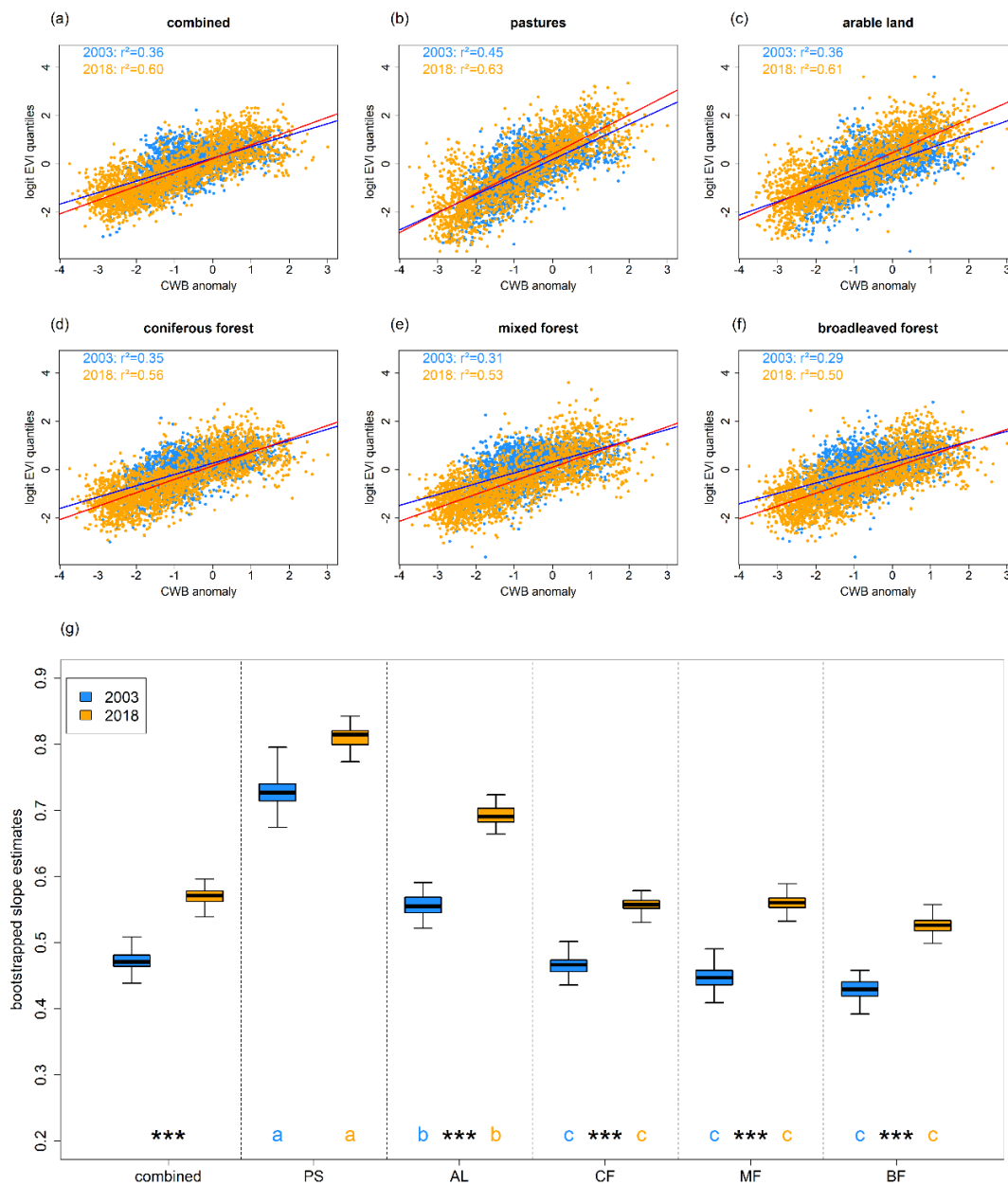
265

Figure 6: Time-series of NDVI-quantiles averaged over the regions featuring CWB < -2 for 2003 (blue) and 2018 (orange) for the five different land-cover classes (b-f) and a combination of those (a).

270 **Figure 7: (a-f) Scatterplots depicting the relationship between average logit-transformed NDVI-quantiles and mean CWB of the 100 CWB percentiles in 2003 (blue) and 2018 (orange) for pastures (b), arable land (c), coniferous forests (d), mixed forest (e), broadleaved forest (f) and a combination of those (a). Blue lines depict the regression line for 2003, red lines for 2018. (g) Bootstrapped regression slope estimates for the five different land-cover classes as well as their combination. Minor case letters refer to group assignment of land-cover classes according to the overlap of 99.9 % confidence intervals of bootstrapped slopes in 2003**

275 **(blue) and 2018 (orange). Significance stars (***) indicate no overlap between 99.9 % confidence intervals of 2003 and 2018 for the respective land-cover class. PS = pastures, AL = arable land, CF = coniferous forest, MF = mixed forest, BF = broadleaved forest. Complementary results for MODIS EVI are shown in supplementary Fig. S7.**

Biogeosciences
Discussions

4 Discussion

4.1 Climatic framework

280 Based on the parameters considered for the quantification of summer conditions, 2018 clearly supersedes the record drought of 2003 (Figs. 1-3). The more persistent anticyclonic circulation patterns for 2018 across Northern Europe as indicated by 500 hPa geopotential height likely triggered the strong positive heat load and negative climatic water balance anomalies across Central and Northern Europe in comparison to 2003.

Anticyclonic blocking situations – as indicated by strong positive 500 hPa geopotential height anomalies – have been reported

285 at an increasing frequency in course of the satellite era (Horton et al., 2015) which likely relates to the increasing persistence of heatwaves observed over the past 60 years (Pfleiderer and Coumou, 2018) and the increasing frequency of a hemisphere-wide wavenumber 7 circulation pattern (Kornhuber et al., 2019). The resulting heatwaves are additionally enhanced by global warming and positive land surface – atmosphere feedback loops via soil moisture depletion and subsequent lack of latent cooling (Fischer et al., 2007). Moreover, summer temperatures and precipitation were reported to correlate negatively at mid

290 latitudes which may amplify further according to CMIP5 climate projections (Zscheischler and Seneviratne, 2017). This renders the evaluation of ecosystem responses to compound events a key topic for climate change research (Zscheischler et al., 2018). Concluding, the prevailing extreme climatic conditions qualify 2018 as a key event for studying ecosystem-responses to hotter droughts in Europe.

4.2 Ecosystem impact

295

4.2.1 Stronger ecosystem impact in 2018

End of July MODIS NDVI anomalies generally supported the impression of a more extreme drought in 2018. That is, the area featuring the lowest quantile in 2018 was twice as high compared to 2003 (Fig. 4c). In accordance with the more northward location of the anticyclone, hotspots of ecosystem impact were concentrated in Central and Northern Europe in 2018.

300 In general, the spatial distribution of NDVI quantiles matches the observed climatic dipole of 2018 very well. Moreover, the bimodal response of European ecosystems is well in line with a report on European maize yield in 2018, with an observed strong increase (10% more than average) for e.g. Romania and Hungary, a strong decrease (10% less than average) for e.g., Germany and Belgium, and the European level net effect estimated at a decrease in maize yield of around 6% (see public references: European Commission).

305 The bimodal behaviour and larger extent of ecosystem impact in 2018 was also reflected in land-cover specific area distributions of NDVI quantiles (Fig. 5a and 5c). That is, the area featuring lowest (highest) quantiles in regions with water deficit (surplus) was much larger in 2018 compared to 2003. Given the skewed distribution of quantiles in those regions, i.e. more lower quantiles in regions with strong negative CWB anomalies and more upper quantiles in regions with strong positive CWB anomalies, the response of these ecosystems appears to be governed by prevailing climate conditions, in particular

310 climatic water balance.

This impression was underlined by linear regressions, which revealed a strong and significant positive impact of CWB on NDVI quantiles in both years and for all land-cover types (Figs. 7a-f). It is noteworthy, that 2018 was characterized by a higher explained variance and significantly more positive model slopes in comparison to 2003 (Fig. 7g). These impressions from single linear models were generally supported by the linear mixed effects model, which showed an increase of r² at about 9 percent when incorporating land-cover and year as random effects.

4.2.2 Location of drought possibly drives stronger ecosystem response in 2018

The stronger coupling (higher r²) between CWB and VI quantiles in 2018 may be related to the period used to integrate CWB (April-July). To test this, we assessed the relationship of VI quantiles with CWB integrated over various different periods (e.g. including previous winter in CWB or shortening the period) which all revealed similar patterns, i.e. a stronger response to CWB in 2018 (not shown). However, it seems possible that the stronger coupling of VI quantiles to CWB in 2018 is related to the spatial distribution of drought and thus the ecosystems being affected. In 2003, the epicenter of the drought was located in Central France and the Mediterranean, i.e. regions which host ecosystems that are regularly experiencing summer drought and thus are likely better adapted to dry conditions. In contrast, the circulation patterns of 2018 resulted in a drought-epicenter in Central Europe, Southern Scandinavia, and around the Baltic Sea, i.e. regions with ecosystems which are less adapted to extremely dry climatic conditions such as in 2018 and therefore likely react strongly. Various reports from dried-out pastures and cornfields as well as deciduous trees shedding their leaves in July and August likely explain the record-low VI values for corresponding Central European ecosystems (see public news references). At the same time, the usually summer-dry Mediterranean experienced water surplus, relaxing the general limitation of the associated ecosystems by plant water availability and leading to a generally higher greenness of the vegetation. Considering forest ecosystems, this interpretation is in line with Klein (2014), who reported higher leaf gas exchange and thus photosynthetic capacity under dry conditions in Mediterranean forests compared to temperate forests. Nevertheless, our hypothesis explaining the stronger coupling of VI quantiles with CWB in 2018 needs further investigation, e.g. by studying the sensitivity and coupling of plant productivity with climatic properties for the considered land-cover classes as for instance done by (Anderegg et al., 2018). A sub-classification of land-cover classes seems to be reasonable for such an analysis, in order to account for possibly differing drought-sensitivities of ecosystems represented by one specific land-cover class. For instance, Mediterranean coniferous forests comprise different species and are thus likely better adapted to drought than boreal coniferous forests in Scandinavia.

4.2.3 Forests featured a weaker immediate response to drought

In addition to the differences between the two drought events, we also observed differing sensitivities of VI quantiles to CWB among ecosystems, which were consistent over the two drought events. We found the highest regression slope estimates for pastures followed by arable land and forests (Fig. 7g). This likely reflects the higher climatic buffering function of forests in comparison to arable land and pastures. In forests, the micro-climate is generally less extreme, leading to lower ambient air temperatures and consequently a lower evapotranspiration in comparison to open fields (Chen et al., 1993, 1999; Young and

345   Mitchell, 1994). Consequently, water resources are consumed more sustainably by forests. Moreover, if not growing on water-logged soils trees typically feature higher rooting depths compared to grasses and crops and therefore have access to deeper soil water reservoirs. Regarding the European drought of 2003, an accelerated soil moisture depletion of grasslands in comparison to forests has been reported earlier (Teuling et al., 2010). Also Wolf et al. (2013) found contrasting responses of grasslands vs. forests regarding water and carbon fluxes during a drought event in 2011. They observed an immediate negative

350   drought-impact on the productivity of managed grasslands while mixed and coniferous forests simply reduced transpiration and maintained GPP, thereby increasing their water-use efficiency and decreasing soil-water consumption (Wolf et al., 2013).

4.2.4 Forest legacy effects

Nevertheless, European forests were in parts heavily affected by the drought 2018, as indicated by the distribution of VI

355   quantiles (Fig. 5c). For instance, 140,000 km² of drought affected coniferous forests featured the lowest quantile in 2018. First estimates for North Rhine-Westphalia (Northwest Germany) assume forest productivity losses of around 40% (see public references: Wald und Holz NRW). Moreover, 20,000 km² of deciduous trees featured the lowest quantile in 2018 which likely relates to the observed early leaf-shedding of deciduous trees in Central Europe (see public-news references). Besides direct impacts, carry-over effects are likely to be experienced in the following years: Evidence for delayed responses comes from

360   remotely sensed vegetation activity in the aftermath of the 2003 event (Reichstein et al., 2007) and reports on observed die-back of Norway spruce, Scots pine, and European beech in spring and summer 2019 (GfÖ-workshop on drought 2018 held on June 4th, 2019 in Basel, see also public news references). These effects could partly be due to legacy effects in tree response to drought (Anderegg et al., 2015; Kannenberg et al., 2018) as well as tree mortality often occurring years after the event (Bigler et al., 2006; Cailleret et al., 2017). Support for an expected delayed response of forests also comes from a severe

365   drought in Franconia, Germany, in 2015, which resulted in increased Scots pine mortality, that was not recognized earlier than in the subsequent winter 2015/2016 and became even more pronounced in spring 2016 (Buras et al., 2018). From this event, we also learned that particularly forest edges – which feature an intermediate micro-climate between the forest interior and open fields – are more susceptible to drought-induced mortality (Buras et al., 2018). However, given the spatial resolution of the applied remote sensing products (231 m x 231 m) patches with tree dieback as well as forest edges could not be resolved,

370   which should therefore be given attention in future studies.

4.3 Call for a European forest monitoring

Given likely legacy effects, studying the development of Central and Northern European forest ecosystems over the next years is particularly interesting and may reveal negative mid- to long-term responses as well as an increased tree mortality. In this

375   context, we propose an immediate observation of forests within the outlined hotspots by combining satellite-based and close-range remote sensing techniques with dendroecological investigations and an eco-physiological monitoring (Buras et al., 2018; Ježík et al., 2015). A timely initiation of such monitoring campaigns would provide the unique opportunity to study natural tree die-back in real-time, thereby increasing our knowledge about drought-induced tree mortality (Cailleret et al., 2017). The

recently released European forest condition monitor (http://www.lsai.wzw.tum.de/index.php?id=71&L=1) may be considered
380   a first step towards a satellite-based, near real-time monitoring of European forests.

5. Conclusions

Based on climatic evidence, 2018 may be considered the new reference year for hotter droughts in Europe. However, the
observed contrasting patterns of the drought events in 2003 and 2018 highlight the complexity of ecosystem responses to
385   severe droughts. More specifically, we observed a different sensitivity of ecosystems to CWB between the two events and a
differing sensitivity of land cover classes to drought, with pastures and agricultural fields expressing a higher sensitivity in
comparison to forests. The observed climatic heterogeneity and resulting ecosystem response poses certain challenges for
estimating the effects on the carbon cycle in European ecosystems in 2018. That is, the observed dipole in 2018 makes it
difficult to directly compare the European carbon budget of 2018 with 2003. Finally, legacy effects of forest ecosystems are
390   likely to occur in course of the next years. Consequently, to obtain a more complete picture about the impact of the drought
2018 we recommend continued satellite-based remote sensing surveys to be accompanied by immediate in-situ monitoring
campaigns. In this context, particular attention should be given to the outlined hotspots of the drought 2018, i.e. Ireland, United
Kingdom, France, Belgium, Luxemburg, the Netherlands, Northern Switzerland, Germany, Denmark, Sweden, Southern
Norway, Czech Republic, Poland, Lithuania, Latvia, Estonia, and Finnland.
395

Data Availability

The datasets analysed for this study are publicly available. Public web-links as well as the post-processing of data is described
in the material and methods section of this article, wherefore all results are reproducible.

400   Author Contributions

AB and CSZ developed the study design. AB conducted all data processing and statistical analyses. Interpretation and
refinement of statistical results was discussed among AB, AR, and CSZ. AB drafted the first version of the article which was
further refined by AR and CSZ.

405   Competing Interests

The authors declare that the research was conducted in the absence of any commercial or financial relationships that could be
construed as a potential conflict of interest.

Acknowledgements

Biogeosciences
Discussions

References

Allen, C. D., Macalady, A. K., Chenchouni, H., Bachelet, D., McDowell, N., Vennetier, M., Kitzberger, T., Rigling, A.,
415   Breshears, D. D., Hogg, E. H. (Ted), Gonzalez, P., Fensham, R., Zhang, Z., Castro, J., Demidova, N., Lim, J.-H., Allard, G.,
Running, S. W., Semerci, A. and Cobb, N.: A global overview of drought and heat-induced tree mortality reveals emerging
climate change risks for forests, For. Ecol. Manag., 259(4), 660–684, doi:10.1016/j.foreco.2009.09.001, 2010.

Allen, C. D., Breshears, D. D. and McDowell, N. G.: On underestimation of global vulnerability to tree mortality and forest
die-off from hotter drought in the Anthropocene, Ecosphere, 6(8), 1–55, doi:10.1890/ES15-00203.1, 2015.

420   Anderegg, W. R. L., Schwalm, C., Biondi, F., Camarero, J. J., Koch, G., Litvak, M., Ogle, K., Shaw, J. D., Shevliakova, E.,
Williams, A. P., Wolf, A., Ziaco, E. and Pacala, S.: Pervasive drought legacies in forest ecosystems and their implications for
carbon cycle models, Science, 349(6247), 528–532, doi:10.1126/science.aab1833, 2015.

Anderegg, W. R. L., Konings, A. G., Trugman, A. T., Yu, K., Bowling, D. R., Gabbitas, R., Karp, D. S., Pacala, S., Sperry, J.
S., Sulman, B. N. and Zenes, N.: Hydraulic diversity of forests regulates ecosystem resilience during drought, Nature,
425   561(7724), 538, doi:10.1038/s41586-018-0539-7, 2018.

Anyamba, A. and Tucker, C. J.: Historical perspective of AVHRR NDVI and vegetation drought monitoring, Remote Sens.
Drought Innov. Monit. Approaches, 23, 2012.

Bastos, A., Ciais, P., Park, T., Zscheischler, J., Yue, C., Barichivich, J., Myneni, R. B., Peng, S., Piao, S. and Zhu, Z.: Was the
extreme Northern Hemisphere greening in 2015 predictable?, Environ. Res. Lett., 12(4), 044016, doi:10.1088/1748-
430   9326/aa67b5, 2017.

Beguería, S. and Vicente-Serrano, S. M.: SPEI: calculation of the standardised precipitation-evapotranspiration index. R
package version 1.6., 2013.

Bigler, C., Bräker, O. U., Bugmann, H., Dobbertin, M. and Rigling, A.: Drought as an Inciting Mortality Factor in Scots Pine
Stands of the Valais, Switzerland, Ecosystems, 9(3), 330–343, doi:10.1007/s10021-005-0126-2, 2006.

435   Breshears, D. D., Cobb, N. S., Rich, P. M., Price, K. P., Allen, C. D., Balice, R. G., Romme, W. H., Kastens, J. H., Floyd, M.
L., Belnap, J., Anderson, J. J., Myers, O. B. and Meyer, C. W.: Regional vegetation die-off in response to global-change-type
drought, Proc. Natl. Acad. Sci. U. S. A., 102(42), 15144–15148, doi:10.1073/pnas.0505734102, 2005.

Buras, A., Schunk, C., Zeiträg, C., Herrmann, C., Kaiser, L., Lemme, H., Straub, C., Taeger, S., Gößwein, S., Klemmt, H.-J.
and Menzel, A.: Are Scots pine forest edges particularly prone to drought-induced mortality?, Environ. Res. Lett. [online]
440   Available from: http://iopscience.iop.org/10.1088/1748-9326/aaa0b4, 2018.

Cailleret, M., Jansen, S., Robert, E. M. R., Desoto, L., Aakala, T., Antos, J. A., Beikircher, B., Bigler, C., Bugmann, H.,
Caccianiga, M., Čada, V., Camarero, J. J., Cherubini, P., Cochard, H., Coyea, M. R., Čufar, K., Das, A. J., Davi, H., Delzon,
S., Dorman, M., Gea-Izquierdo, G., Gillner, S., Haavik, L. J., Hartmann, H., Hereş, A.-M., Hultine, K. R., Janda, P., Kane, J.
M., Kharuk, V. I., Kitzberger, T., Klein, T., Kramer, K., Lens, F., Levanic, T., Linares Calderon, J. C., Lloret, F., Lobo-Do-
445   Vale, R., Lombardi, F., López Rodríguez, R., Mäkinen, H., Mayr, S., Mészáros, I., Metsaranta, J. M., Minunno, F., Oberhuber,
W., Papadopoulos, A., Peltoniemi, M., Petritan, A. M., Rohner, B., Sangüesa-Barreda, G., Sarris, D., Smith, J. M., Stan, A.
B., Sterck, F., Stojanović, D. B., Suarez, M. L., Svoboda, M., Tognetti, R., Torres-Ruiz, J. M., Trotsiuk, V., Villalba, R.,
Vodde, F., Westwood, A. R., Wyckoff, P. H., Zafirov, N. and Martínez-Vilalta, J.: A synthesis of radial growth patterns
preceding tree mortality, Glob. Change Biol., 23(4), 1675–1690, doi:10.1111/gcb.13535, 2017.

450   Chen, J., Franklin, J. F. and Spies, T. A.: Contrasting microclimates among clearcut, edge, and interior of old-growth Douglas-fir forest, Agric. For. Meteorol., 63(3), 219–237, doi:10.1016/0168-1923(93)90061-L, 1993.

Chen, J., Saunders, S. C., Crow, T. R., Naiman, R. J., Brosofske, K. D., Mroz, G. D., Brookshire, B. L. and Franklin, J. F.: Microclimate in Forest Ecosystem and Landscape EcologyVariations in local climate can be used to monitor and compare the effects of different management regimes, BioScience, 49(4), 288–297, doi:10.2307/1313612, 1999.

455   Choat, B., Brodribb, T. J., Brodersen, C. R., Duursma, R. A., López, R. and Medlyn, B. E.: Triggers of tree mortality under drought, Nature, 558(7711), 531–539, doi:10.1038/s41586-018-0240-x, 2018.

Ciais, P., Reichstein, M., Viovy, N., Granier, A., Ogée, J., Allard, V., Aubinet, M., Buchmann, N., Bernhofer, C., Carrara, A., Chevallier, F., Noblet, N. D., Friend, A. D., Friedlingstein, P., Grünwald, T., Heinesch, B., Keronen, P., Knohl, A., Krinner, G., Loustau, D., Manca, G., Matteucci, G., Miglietta, F., Ourcival, J. M., Papale, D., Pilegaard, K., Rambal, S., Seufert, G.,
460   Soussana, J. F., Sanz, M. J., Schulze, E. D., Vesala, T. and Valentini, R.: Europe-wide reduction in primary productivity caused by the heat and drought in 2003, Nature, 437(7058), 529–533, doi:10.1038/nature03972, 2005.

Fink, A. H., Brücher, T., Krüger, A., Leckebusch, G. C., Pinto, J. G. and Ulbrich, U.: The 2003 European summer heatwaves and drought –synoptic diagnosis and impacts, Weather, 59(8), 209–216, doi:10.1256/wea.73.04, 2004.

Fischer, E. M., Seneviratne, S. I., Vidale, P. L., Lüthi, D. and Schär, C.: Soil Moisture–Atmosphere Interactions during the
465   2003 European Summer Heat Wave, J. Clim., 20(20), 5081–5099, doi:10.1175/JCLI4288.1, 2007.

García-Herrera, R., Díaz, J., Trigo, R. M., Luterbacher, J. and Fischer, E. M.: A review of the European summer heat wave of 2003, Crit. Rev. Environ. Sci. Technol., 40(4), 267–306, 2010.

Hargreaves, G. H.: Defining and Using Reference Evapotranspiration, J. Irrig. Drain. Eng., 120(6), 1132–1139, doi:10.1061/(ASCE)0733-9437(1994)120:6(1132), 1994.

470   Hijmans, R. J.: raster: Geographic Data Analysis and Modeling, 2017.

Horton, D. E., Johnson, N. C., Singh, D., Swain, D. L., Rajaratnam, B. and Diffenbaugh, N. S.: Contribution of changes in atmospheric circulation patterns to extreme temperature trends, Nature, 522(7557), 465–469, doi:10.1038/nature14550, 2015.

Huete, A. R., Didan, K., Shimabukuro, Y. E., Ratana, P., Saleska, S. R., Hutyra, L. R., Yang, W., Nemani, R. R. and Myneni, R.: Amazon rainforests green-up with sunlight in dry season, Geophys. Res. Lett., 33(6), doi:10.1029/2005GL025583, 2006.

475   IPCC: Climate change 2014: synthesis report. Contribution of Working Groups I, II and III to the fifth assessment report of the Intergovernmental Panel on Climate Change, IPCC., 2014.

Ježík, M., Blaženec, M., Letts, M. G., Ditmarová, Ľ., Sitková, Z. and Střelcová, K.: Assessing seasonal drought stress response in Norway spruce (Picea abies (L.) Karst.) by monitoring stem circumference and sap flow, Ecohydrology, 8(3), 378–386, doi:10.1002/eco.1536, 2015.

480   Kalnay, E., Kanamitsu, M., Kistler, R., Collins, W., Deaven, D., Gandin, L., Iredell, M., Saha, S., White, G., Woollen, J., Zhu, Y., Chelliah, M., Ebisuzaki, W., Higgins, W., Janowiak, J., Mo, K. C., Ropelewski, C., Wang, J., Leetmaa, A., Reynolds, R., Jenne, R. and Joseph, D.: The NCEP/NCAR 40-Year Reanalysis Project, Bull. Am. Meteorol. Soc., 77(3), 437–472, doi:10.1175/1520-0477(1996)077<0437:TNYRP>2.0.CO;2, 1996.

Kannenberg, S. A., Maxwell, J. T., Pederson, N., D'Orangeville, L., Ficklin, D. L. and Phillips, R. P.: Drought legacies are
485 dependent on water table depth, wood anatomy and drought timing across the eastern US, Ecol. Lett., doi:10.1111/ele.13173,
2018.

Klein, T.: The variability of stomatal sensitivity to leaf water potential across tree species indicates a continuum between
isohydric and anisohydric behaviours, Funct. Ecol., 28(6), 1313–1320, doi:10.1111/1365-2435.12289, 2014.

Kornhuber, K., Osprey, S., Coumou, D., Petri, S., Petoukhov, V., Rahmstorf, S. and Gray, L.: Extreme weather events in early
490 summer 2018 connected by a recurrent hemispheric wave-7 pattern, Environ. Res. Lett., 14(5), 054002, doi:10.1088/1748-
9326/ab13bf, 2019.

Matusick, G., Ruthrof, K. X., Kala, J., Brouwers, N. C., Breshears, D. D. and Hardy, G. E. S. J.: Chronic historical drought
legacy exacerbates tree mortality and crown dieback during acute heatwave-compounded drought, Environ. Res. Lett., 13(9),
095002, doi:10.1088/1748-9326/aad8cb, 2018.

495 Misra, G., Buras, A. and Menzel, A.: Effects of different methods on the comparison between land surface and ground
phenology—A methodological case study from south-western Germany, Remote Sens., 8(9), 753, 2016.

Misra, G., Buras, A., Heurich, M., Asam, S. and Menzel, A.: LiDAR derived topography and forest stand characteristics largely
explain the spatial variability observed in MODIS land surface phenology, Remote Sens. Environ., 218, 231–244,
doi:10.1016/j.rse.2018.09.027, 2018.

500 Myneni, R. B., Hall, F. G., Sellers, P. J. and Marshak, A. L.: The interpretation of spectral vegetation indexes, IEEE Trans.
Geosci. Remote Sens., 33(2), 481–486, 1995.

Orth, R., Zscheischler, J. and Seneviratne, S. I.: Record dry summer in 2015 challenges precipitation projections in Central
Europe, Sci. Rep., 6, 28334, doi:10.1038/srep28334, 2016.

Pfleiderer, P. and Coumou, D.: Quantification of temperature persistence over the Northern Hemisphere land-area, Clim. Dyn.,
505 51(1–2), 627–637, doi:10.1007/s00382-017-3945-x, 2018.

Pinheiro, J., Bates, D., DebRoy, S., Sarkar, D., Heisterkamp, S., Van Willigen, B. and Maintainer, R.: Package 'nlme,' Linear
Nonlinear Mix. Eff. Models Version, 3–1, 2017.

R core team: R: A language and environment for statistical computing, 2019. R foundation for Statistical Computing, Vienna,
Austria.

510 Seneviratne, S. I., Corti, T., Davin, E. L., Hirschi, M., Jaeger, E. B., Lehner, I., Orlowsky, B. and Teuling, A. J.: Investigating
soil moisture–climate interactions in a changing climate: A review, Earth-Sci. Rev., 99(3), 125–161,
doi:10.1016/j.earscirev.2010.02.004, 2010.

Sippel, S., Forkel, M., Rammig, A., Thonicke, K., Flach, M., Heimann, M., Otto, F. E. L., Reichstein, M. and Mahecha, M.
D.: Contrasting and interacting changes in simulated spring and summer carbon cycle extremes in European ecosystems,
515 Environ. Res. Lett., 12(7), 075006, doi:10.1088/1748-9326/aa7398, 2017.

Teuling, A. J., Seneviratne, S. I., Stöckli, R., Reichstein, M., Moors, E., Ciais, P., Luyssaert, S., van den Hurk, B., Ammann,
C., Bernhofer, C., Dellwik, E., Gianelle, D., Gielen, B., Grünwald, T., Klumpp, K., Montagnani, L., Moureaux, C.,
Sottocornola, M. and Wohlfahrt, G.: Contrasting response of European forest and grassland energy exchange to heatwaves,
Nat. Geosci., 3(10), 722–727, doi:10.1038/ngeo950, 2010.

520 Thornthwaite, C. W.: An Approach toward a Rational Classification of Climate, Geogr. Rev., 38(1), 55–94, doi:10.2307/210739, 1948.

Wolf, S., Eugster, W., Ammann, C., Häni, M., Zielis, S., Hiller, R., Stieger, J., Imer, D., Merbold, L. and Buchmann, N.: Contrasting response of grassland versus forest carbon and water fluxes to spring drought in Switzerland, Environ. Res. Lett., 8(3), 035007, doi:10.1088/1748-9326/8/3/035007, 2013.

525 Xu, L., Samanta, A., Costa, M. H., Ganguly, S., Nemani, R. R. and Myneni, R. B.: Widespread decline in greenness of Amazonian vegetation due to the 2010 drought, Geophys. Res. Lett., 38(7), doi:10.1029/2011GL046824, 2011.

Young, A. and Mitchell, N.: Microclimate and vegetation edge effects in a fragmented podocarp-broadleaf forest in New Zealand, Biol. Conserv., 67(1), 63–72, doi:10.1016/0006-3207(94)90010-8, 1994.

Zscheischler, J. and Seneviratne, S. I.: Dependence of drivers affects risks associated with compound events, Sci. Adv., 3(6),
530 e1700263, doi:10.1126/sciadv.1700263, 2017.

Zscheischler, J., Westra, S., van den Hurk, B. J. J. M., Seneviratne, S. I., Ward, P. J., Pitman, A., AghaKouchak, A., Bresch, D. N., Leonard, M., Wahl, T. and Zhang, X.: Future climate risk from compound events, Nat. Clim. Change, 8(6), 469–477, doi:10.1038/s41558-018-0156-3, 2018.

535 **Public news references**

https://www.climate.gov/news-features/event-tracker/hot-dry-summer-has-led-drought-europe-2018 (in English).

https://www.euronews.com/2018/08/10/explained-europe-s-devastating-drought-and-the-countries-worst-hit (in English).
Short-term outlook of the European Commission for EU agricultural markets: https://ec.europa.eu/agriculture/markets-and-
540 prices/short-term-outlook_en (in English).

MODIS-based maps on land surface temperature and cloud cover anomalies for whole Europe: https://www.geografiainfinita.com/2018/09/un-analisis-de-la-sequia-en-europa-en-el-verano-de-2018/?platform=hootsuite (in Spanish).
545
German atlas for soil water depletion, provided by the Umwelt-Forschungs-Zentrum UFZ: https://www.ufz.de/index.php?de=44429 (in German).

Report on the impacts of the heat-wave in Germany, provided by the Karlsruhe Institute of Technology KIT:
550 http://www.kit.edu/kit/pi_2018_102_durre-betrifft-rund-90-prozent-der-flache-deutschlands.php (in German).

Interim report of ‚Wald und Holz NRW‘ on the impacts of the drought 2018 on forest productivity in North-Rhine Westphalia: https://www.wald-und-holz.nrw.de/aktuelle-meldungen/2018/zwischenbilanz-trockensommer-2018 (in German).

555 Pictures from dried-out cornfields in Germany: https://www.alamy.com/corn-field-dried-up-and-only-grown-low-small-corn-cobs-through-the-summer-drought-drought-in-ostwestfalen-lippe-germany-summer-2018-image215773502.html

Report on early leaf shedding of deciduous trees in Germany: https://www.wetteronline.de/wetternews/trockenheit-setzt-natur-zu-viele-baeume-werfen-ihr-laub-ab-2018-08-14-lb (in German)

560

New insights on the impacts of the drought 2018 in Switzerland: https://www.wsl.ch/de/ueber-die-wsl/programme-und-initiativen/wsl-initiative-trockenheit-2018/c2-gruen-waldbedachung.html (in German).

Beech die-back in the Hainich national park in Germany: https://www.nationalpark-hainich.de/de/aktuelles/aktuelles-
565 presse/einzelansicht/extremjahr-2018-hinterlaesst-spuren-im-nationalpark-hainich.html (in German).